Wiley Online Library
Early View publication on www.wileyonlinelibrary.com
(issue and page numbers not yet assigned;
citable using Digital Object Identifier – **DOI**)

Phys. Status Solidi C, 1700103 (2017) / **DOI** 10.1002/pssc.201700103

physica status solidi c
www.pss-c.com
current topics in solid state physics

Characterization of light-activated Cu defects in silicon: Comparison with the recombination activity of metallic precipitates

Alessandro Inglese*[,1], Henri Vahlman[1], Wolfram Kwapil[2], Jonas Schön[2], and Hele Savin[1]

[1] Department of Electronics and Nanoengineering, Aalto University, 02150 Espoo, Finland
[2] Fraunhofer Institute for Solar Energy Systems ISE, Heidenhofstraße 2, 79110 Freiburg im Breisgau, Germany

Received 28 February 2017, accepted 7 April 2017
Published online 28 April 2017

Keywords copper impurities, Cu-LID, defect characterization, metal precipitates, silicon

* Corresponding author: e-mail alessandro.inglese@aalto.fi, Phone: +358 50 431 6367

The presence of copper contamination is known to severely degrade the minority carrier lifetime of p-type silicon upon exposure to illumination. In this contribution, we have analyzed the recombination activity of light-activated copper defects in deliberately Cu-contaminated p-type silicon by means of a recombination model that quantitatively defines the effect of metallic precipitates on minority carrier lifetime. The excellent agreement between the model and the experimental data indicates that (i) the formation of Cu precipitates is the probable root-cause behind Cu-LID and (ii) in the samples examined in this work, the precipitate radius varies between few to several tens of nm with corresponding densities estimated to be in the range of 10^8–10^{10} cm^{-3}. Further evidence of these results was obtained from the analysis of temperature-dependent lifetime data. While applied here to light-activated copper defects, the procedure described in this article can be applied for characterizing lifetime-limiting precipitates originated by other transition metals (e.g., Fe or Ni).

1 Introduction Copper is a common *3d* metal impurity in silicon, which produces adverse effects on the operation of state-of-the-art solar cells [1]. Low levels of copper contamination have been shown to severely degrade the minority carrier lifetime in p-type silicon upon exposure to illumination [2–4], thereby impacting the stability of solar cell efficiency during light soaking. This phenomenon, which is referred in literature to as copper-related light-induced degradation (Cu-LID), has been associated to the transformation of recombination-inactive interstitial copper atoms (Cu_i^+) into a different lifetime limiting defect [5]. However, the mechanisms behind Cu-LID and the defect generated during the degradation process still remain a matter of investigation [6]. In a recent contribution, the recombination activity of light-activated copper defects has been studied in terms of Shockley–Read–Hall (SRH) recombination statistics through lifetime spectroscopy methods [7]. The analysis indicated the coexistence of at least two energy levels, i.e., a deep energy state located near the mid-bandgap and a shallow level in the upper bandgap half, which approximately correspond to the boundaries of the energy range associated to Cu precipitates [8]. Nevertheless, considering the extended nature of metallic precipitates, a rigorous study of carrier recombination at these defects requires the use of more advanced models than simple SRH statistics. A more suitable approach to estimate the impact of metallic precipitates on minority carrier lifetime would be e.g., the model introduced by Plekhanov and Tan [9], which was specifically developed to describe the carrier recombination mechanisms at metallic precipitates.

In the following, the injection and temperature-dependent lifetime results have been analyzed by means of this recombination model. This contribution extends and consolidates the previous studies on the recombination activity of light-activated copper defects. In addition, this work serves as an example of application of this recombination model to complement the existing lifetime spectroscopy methods [10, 11] with the identification and characterization of metallic precipitates.

2 Sample preparation and lifetime measurements The experiments were performed with Czochralski (Cz-) and Float-Zone (FZ-) Si wafers with resistivities of 3.4 and 1.1 Ω·cm, respectively, and thicknesses of 380 ± 10 μm and 250 ± 15 μm. In the Cz-Si sample, the interstitial oxygen concentration was >14 ppma.

All samples were thermally oxidized at 900 °C in O_2 for 40 min, followed by a 20 min anneal in nitrogen ambient. Bulk Cu contamination was performed with the spin-on method, followed by in-diffusion at 800 °C in inert ambient. The interstitial Cu concentration (N_{Cu_i}) after in-diffusion was estimated to be around 1.0×10^{14} cm^{-3} for the Cz sample and 1.6×10^{14} cm^{-3} for the FZ sample [12].

After a +260 nC/cm^2 corona charge deposition on both wafer surfaces, the samples were degraded under 0.65 Suns illumination at room temperature (RT) for about 100 h. The lifetime decay was constantly recorded as a function of illumination time through the quasi-steady state photoconductance decay (QSSPC) method performed with a Sinton WCT 120-TS lifetime tester [13, 14]. The same technique was utilized for the temperature-dependent measurements, which were performed by heating the measurement stage up to 200 °C and subsequently acquiring the data during the cooling transient.

3 Modeling of recombination at metallic precipitates The recombination model is based upon the assumption that the dominant physical mechanism is the generation of thermionic emission currents due to a Schottky junction between the silicide (Cu precipitate – which exists in Si in the form of Cu_3Si silicides [15]) and the surrounding semiconductor [9]. In this model, the metal precipitate is assumed to be spherical and the extent of the space charge region (SCR) around the silicide is imposed by the junction electric field. Since the excess carrier concentration (Δn), the radius of the metallic precipitate (r_{prec}) and semiconductor doping (N_a) considerably influence the electric fields at the junction (and therefore the width of the SCR), all these parameters ultimately impact the precipitate-related capture cross section.

The quantitative description of precipitate-related recombination as a function of the excess carrier concentration, in general, requires the execution of finite-element simulations, where the continuity equations for holes and electrons are solved together with the Poisson equation. The carrier recombination rate is then calculated by integrating the thermionic emission currents over the silicide/semiconductor interface and averaging over the simulation domain. In order to ease the determination of the precipitate-limited lifetime, Kwapil et al. proposed a parametrization of the numerical results which allows to quickly calculate the injection-dependent lifetime, without the need of numerical simulations. This parametrization consists of a set of equations which estimate the dependence of the precipitate capture cross section (σ_{prec}) on the input parameters, i.e., N_a, Δn and the precipitate radius r_{prec}. The precipitate-related lifetime is then calculated as follows:

$$\tau_{prec} = \frac{1}{N_{prec}(r_{prec})\sigma_{prec}(\Delta n,\ r_{prec},\ N_a)v_{th}} \quad (1)$$

where N_{prec} is the density of precipitates with radius r_{prec} and v_{th} represents the carrier thermal velocity (10^7 cm/s [11]). Full description of the model and the associated parametrization can be found in Refs. [16] and [17].

4 Results and discussion

4.1 Degradation process Figure 1 presents the effective lifetime measured during room-temperature illumination in intentionally Cu-contaminated samples. It can be observed that, while in the FZ-specimen the LID effect becomes visible after several tens of minutes, in the Cz-sample the degradation occurs upon exposure to illumination. In order to distinguish the effect of Cu-LID from the boron-oxygen defect (fast and slow components) [18] in the Cz-sample, an identical uncontaminated Cz-wafer has been degraded under the same light source. It turns out that in the Cu-contaminated Cz-sample the initial phase of degradation is dominated by BO-LID (up to ~1 min of illumination), whereas the later stages are clearly caused by the formation of light-activated Cu defects. Hence, from the data plotted in Fig. 1 the Cu-LID process in the Cz-Si specimen appears to be considerably faster than in the FZ-Si sample. In the following sections, the defect characterization by means of the Schottky model has been performed on the lifetime data measured after approximately 100 h of uninterrupted illumination, which led to the saturation of the Cu-related lifetime degradation process in both specimens.

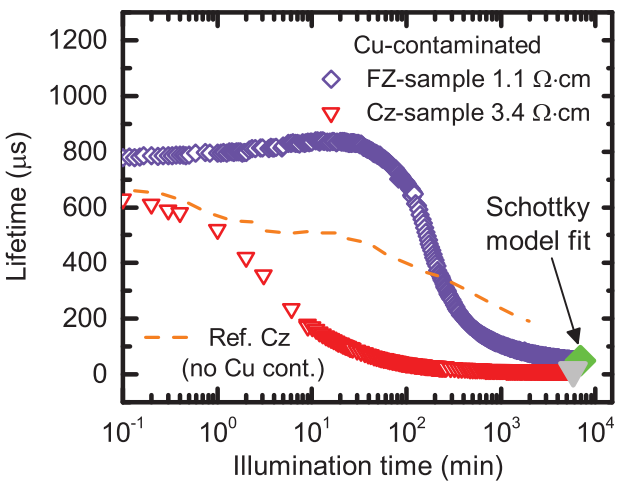

Figure 1 Effective lifetime measured as a function of illumination time at fixed injection level $\Delta n = 0.1 \times N_a$ in Cu-contaminated Cz-Si sample and the FZ-Si sample (purple squares). The dashed line represents the lifetime decay measured with a reference uncontaminated Cz-specimen, whose degradation is solely determined by the light-induced activation of the boron-oxygen complex.

4.2 Fit of injection-dependent lifetime data For the correct analysis of the injection-dependent lifetime data through the Schottky model, the Cu-related lifetime must be separated from the effect of the BO-complex and other recombination channels (e.g., Auger, intrinsic and surface recombination). Figure 2 shows the lifetime related to the light-activated Cu defects (τ_{Cu}), that was calculated by compensating the reciprocal of the effective lifetime measured after degradation (τ_{deg}) with the lifetime curve measured before light soaking (τ_{init}). In the case of the Cz-sample, an additional correction was necessary to subtract the effect of the BO-complex. This was done by compensating τ_{Cu} with the injection-dependent lifetime measured after illumination in a reference uncontaminated sample (τ_{BO}). The superposition of the curves representing ($\tau_{Cu}^{FZ/Cz}$) and τ_{deg} over the whole injection range proves that the measured lifetime is largely dominated by the recombination strength of the light-activated Cu defects.

In Fig. 3a, the parametrization of the Schottky model has been fitted to $\tau_{Cu}(\Delta n)$ with the least squares method assuming that, after LID, the interstitial Cu concentration (N_{Cu_i}) reported in Section 2 has fully transformed into the recombination active precipitated form. In addition, the fit has been performed under the assumption that all precipitates feature the same size. In other words, for the determination of the precipitate-related lifetime, the entire amount of interstitial Cu atoms has been presumed to transform into precipitates whose size corresponds to an average value. Given these assumptions, the precipitate density N_{prec} of Eq. (1) becomes fixed and it can be written as a function of r_{prec} as follows:

$$N_{prec}(r_{prec}) = \frac{N_{Cu_i}}{\rho_{Cu} V_{prec}(r_{prec})}, \quad (2)$$

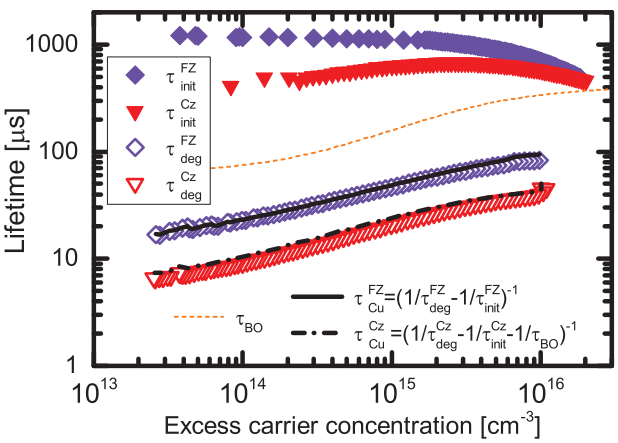

Figure 2 Injection-dependent lifetime curves measured before and after illumination (symbols). Also shown in the image are the effective Cu-related lifetime curves (τ_{Cu}^{FZ} and τ_{Cu}^{Cz}) calculated by compensating τ_{deg} with τ_{init} and τ_{BO}.

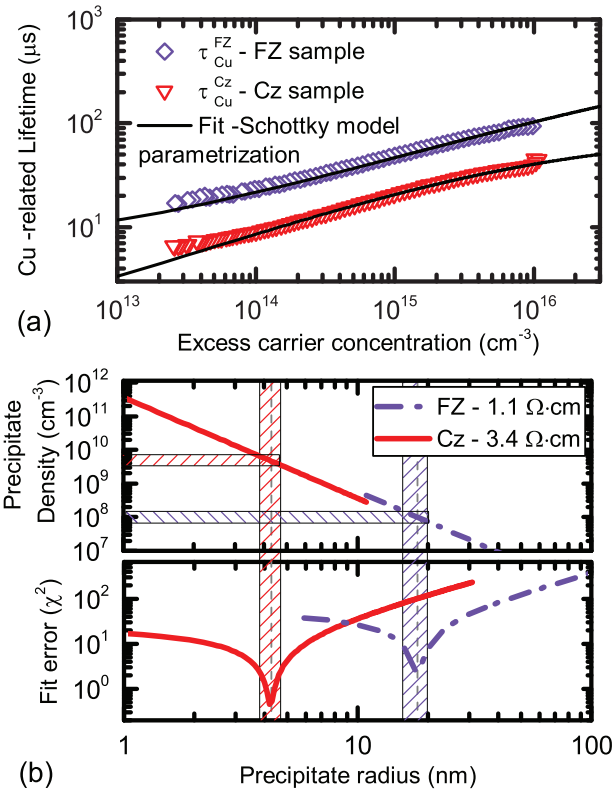

Figure 3 (a) Least squares fit of the injection-dependent Cu-related lifetime. The parameters that provide the best fit to the experimental data are shown in (b) where the precipitate density and the corresponding fit error (χ^2) have been calculated for each value of the precipitate radius. The shaded areas define the values of the precipitate radii/densities that minimize the fit error.

where $\rho_{Cu} = 6.52 \times 10^{22}\,cm^{-3}$ is the density of Cu atoms in each precipitate [19, 20] and $V_{prec} = 4/3\pi r_{prec}^3$ is the precipitate spherical volume.

Although the aforementioned assumptions surely represent an approximation of the real precipitate size distributions, Fig. 3a shows that excellent agreement between the injection-dependent curves predicted by the model and the experimental data. In Fig. 3b, the goodness of fit has been quantified in terms of mean squared sum of residuals (χ^2) for predefined values of precipitate radius/density. It can be observed that in the case of the Cz-specimen with lower resistivity, the optimum fit is obtained with a precipitate radius of ~20 nm and a density of $\sim 1 \times 10^8\,cm^{-3}$. On the other hand, the best fit to the lifetime data acquired with the FZ-sample indicates the presence of precipitates with smaller radius ($r_{prec} \sim 4$ nm) and higher density ($N_{prec} \sim 4 \times 10^9\,cm^{-3}$).

On the base of the results presented in Figs. 1 and 3, it can be concluded that the slower degradation rate observed in the FZ-Si sample leads to the formation of larger precipitates than the Cz-Si specimen. On the other hand, in the Cz-sample the Cu-LID process is accompanied by the formation of precipitates featuring a smaller radius and capture cross section. In this case, the considerable increase

in estimated precipitate density with respect to the FZ-sample overcompensates the weaker recombination activity of each single precipitate arising from the smaller capture cross section.

Despite the initial simplifying assumption (i.e., the same size for all precipitates), the fitted precipitate radii and densities are in good agreement with the simulated precipitate size distributions reported in Ref. [18]. Hence, the excellent fit to the experimental data in Fig. 3a and the correspondence of the fitted precipitate radii/densities with the results in Ref. [18] strengthen the hypothesis of Cu-precipitation being the root-cause behind the observed LID.

As previously mentioned, the precipitation of Cu impurities has been extensively investigated in recent contributions [12, 18] which presented a comprehensive mathematical model to describe the underlying mechanisms. According to this model, the Cu-precipitation rate is regulated by the solubility of Cu_i atoms. Higher doping concentrations decrease the supersaturation level of Cu_i atoms, which represents the main driving force for Cu precipitation kinetics. Hence, the higher doping level of the FZ-specimen imposes a lower supersaturation level of Cu_i atoms, which slows down the nucleation rate for Cu precipitates and eventually results in the formation of larger precipitates. Heavy B-doping is also known to lower the diffusivity of Cu_i^+ atoms due to Cu-B pairing [19]. However, this phenomenon was shown to play a minor effect on the overall doping dependence of Cu precipitation kinetics.

Another factor that might play a role in the different Cu-related degradation rates and precipitate size/density is the possible formation of oxygen precipitates in the Cz-sample during oxidation and the subsequent thermal anneals for in-diffusing Cu impurities. Such oxygen precipitates were shown to remarkably accentuate and accelerate the Cu-LID effects [21].

4.3 Analysis of temperature-dependent lifetime data In order to further ascertain the agreement between the model and the experimental data, the Schottky model was applied to temperature-dependent lifetime data measured at fixed injection level. As no parametrization exists for modeling the recombination at higher temperatures than 300 K, the lifetime temperature dependence must be calculated through finite element simulations based on the Schottky model [9, 16].

Figure 4 plots the simulated lifetime together with the experimental data detected across the measurable temperature range (300–470 K) at the excess carrier concentration of $2 \times 10^{14}\,cm^{-3}$. The simulated points were calculated assuming the previously determined precipitate radii and densities. In the figure, it can be observed that good agreement exists between the experimental data and the simulated values.

Since all the experimental points in Fig. 3 were measured at fixed injection level and no significant dissolution of Cu precipitates is likely to occur at

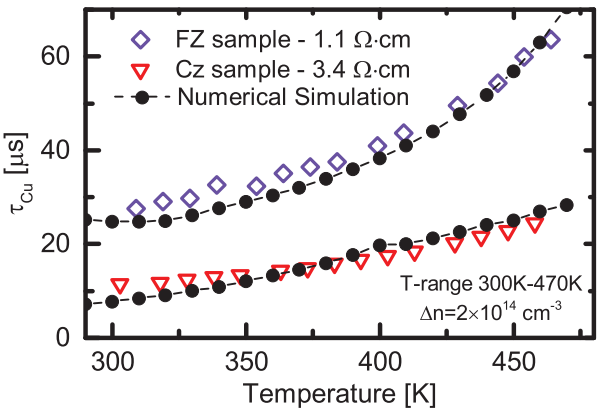

Figure 4 Experimental (open symbols) and simulated (filled circles) lifetime data plotted as a function of temperature. The experimental data were measured at the excess carrier concentration of $2 \times 10^{14}\,cm^{-3}$ and numerical simulations were based on the recombination model described in Section 3.

temperatures below 200 °C [6], on the base of Eq. (1) the variation of the measured lifetime as a function of the temperature may only originate from the temperature-dependence of the minority carrier capture cross section σ_{prec} and the thermal velocity v_{th}. As v_{th} monotonically increases with temperature [11], the upward trend of the measured lifetime at higher temperatures suggests that the capture cross section becomes smaller at increasing temperatures. Specifically, the increase in measured lifetime as a function of temperature suggests that the shrinkage of the capture cross section at higher temperature over-compensates the increase in v_{th}. This result is consistent with the SRH-based analysis presented in Ref. [7], where a good fit to the experimental lifetime data could only be obtained under the assumption of a power-law temperature dependence ($\sigma \sim T^{-\alpha}$) of capture cross sections.

In addition to the effect of temperature and excess carrier concentration on capture cross sections, other phenomena, which were not taken into account in the numerical simulation, may also affect the precipitate-related recombination. For example, charge states exist at the metal/semiconductor interface [9], which increase the interface recombination velocity and, therefore, the overall precipitate-related recombination activity. The augmented thermionic emission at higher temperatures may cause the occupation of such states by the thermally generated carriers, thus reducing the recombination rate at the precipitate. It is, however, questionable whether such phenomenon plays a significant role at temperatures below 200 °C.

Another phenomenon worth mentioning is the possible occurrence of tunneling effects in sub 10 nm precipitates, which was hypothesized in Ref. [22] to define the recombination strength of molybdenum nanoprecipitates. This effect was shown to significantly enhance the majority carrier capture rate due to the increased sharpness of the band bending at the Schottky junction. However, the impact of such phenomenon on the minority capture cross sections

still needs to be quantified and, therefore, further studies are needed to determine whether such tunneling play any role in the results presented above.

5 Conclusions The results presented in this work have shed some new light on the defect causing Cu-LID. The injection and temperature-dependent lifetime data measured with intentionally contaminated wafers have been analyzed by means of a model that quantitatively calculates the carrier recombination at metallic precipitates. The excellent agreement between model and the injection/temperature-dependent lifetime data confirms that Cu precipitates are the probable root-cause behind Cu-LID. The analysis of the experimental data also provided an estimate of the size and density of these precipitates. Particularly, the fitted precipitate radii in the samples used for this study resulted to be in the range of few to several tens of nm and the corresponding density was found to vary between 10^8 and $10^{10}\,cm^{-3}$. For further confirmation, future studies may include electrical characterization via DLTS and high resolution imaging through microscopy techniques (e.g., SIRM or TEM).

Besides providing evidence of Cu precipitates being the defect responsible of Cu-LID, this work serves as an example of application of the Schottky model for the identification and characterization of metallic precipitates. While SRH statistics are well suited for describing carrier recombination at point defects, their application to extended defects leaves behind a certain degree of ambiguity on the exact nature of the underlying defect. This contribution demonstrates that additional information can be gained by complementing SRH-based lifetime spectroscopy analyses with more advanced recombination models.

Acknowledgements The work has been funded by the European Research Council under the European Union's FP7 Programme ERC Grant Agreement No. 307315 (SolarX project). The authors acknowledge the provision of facilities and technical support by Aalto University at the Micronova Nanofabrication Centre. A.I. also acknowledges the financial support of Aalto ELEC doctoral school and Alfred Kordelin Foundation.

References

[1] T. Turmagambetov, S. Dubois, J.-P. Garandet, B. Martel, N. Enjalbert, J. Veirman, and E. Pihan, Phys. Status Solidi (c) **11**, 1697 (2014).
[2] H. Savin, M. Yli-Koski, and A. Haarahiltunen, Appl. Phys. Lett. **95**, 152111 (2009).
[3] A. Inglese, J. Lindroos, and H. Savin, Appl. Phys. Lett. **107**, 052101 (2015).
[4] A. Inglese, A. Focareta, F. Schindler, J. Schön, J. Lindroos, M. C. Schubert, and H. Savin, Energy Procedia **92**, 808–814 (2016).
[5] A. Belayachi, T. Heiser, J. P. Schunck, and A. Kempf, Appl. Phys. A **80**, 201 (2005).
[6] J. Lindroos and H. Savin, Sol. Energy Mater. Sol. Cells **147**, 115–126 (2016).
[7] A. Inglese, J. Lindroos, H. Vahlman, and H. Savin, J. Appl. Phys. **120**, 125703 (2016).
[8] M. Seibt, R. Khalil, V. Kveder, and W. Schröter, Appl. Phys. A **96**, 235 (2009).
[9] P. S. Plekhanov and T. Y. Tan, Appl. Phys. Lett. **76**, 3777 (2000).
[10] S. Rein, Lifetime Spectroscopy (Springer-Verlag, Berlin/Heidelberg, 2005).
[11] S. Rein, T. Rehrl, W. Warta, and S. W. Glunz, J. Appl. Phys. **91**, 2059 (2002).
[12] H. Vahlman, A. Haarahiltunen, W. Kwapil, J. Schön, A. Inglese, and H. Savin (submitted).
[13] B. B. Paudyal, K. R. McIntosh, D. H. Macdonald, B. S. Richards, and R. A. Sinton, Prog. Photovoltaics Res. Appl. **16**, 609 (2008).
[14] R. A. Sinton, A. Cuevas, and M. Stuckings, in *Conf. Rec. 25th IEEE Photovolt. Spec. Conf. – 1996* (IEEE, 1996), pp. 457–460.
[15] W. Schröter, V. Kveder, M. Seibt, H. Ewe, H. Hedemann, F. Riedel, and A. Sattler, Mater. Sci. Eng. B **72**, 80 (2000).
[16] W. Kwapil, J. Schon, F. Schindler, W. Warta, and M. C. Schubert, IEEE J. Photovoltaics **4**, 791–798 (2014).
[17] W. Kwapil, J. Schon, W. Warta, and M. C. Schubert, IEEE J. Photovoltaics **5**, 1285–1292 (2015).
[18] H. Vahlman, A. Haarahiltunen, W. Kwapil, J. Schön, A. Inglese, and H. Savin (submitted).
[19] A. A. Istratov and E. R. Weber, J. Electrochem. Soc. **149**, G21 (2002).
[20] M. Yli-Koski, *Optical Activation of Copper in Silicon Studied by Carrier Lifetime Measurements* (Doctoral dissertation – Helsinki University of Technology, 2004).
[21] H. Väinölä, M. Yli-Koski, A. Haarahiltunen, and J. Sinkkonen, J. Electrochem. Soc. **150**, G790 (2003).
[22] J. Jacobs, B. Hamilton, S. Leonard, V. P. Markevich, and A. R. Peaker, in *2015 IEEE 42nd Photovolt. Spec. Conf.* (IEEE, 2015), pp. 1–3.